



Frictional sliding in serpentine at very high pressure

Haemyeong Jung^{a,b,c,d,*}, Yingwei Fei^b, Paul G. Silver^c, Harry W. Green II^a

^a Institute of Geophysics and Planetary Physics and Department of Earth Sciences, University of California, Riverside, CA 92521, USA

^b Geophysical Laboratory, Carnegie Institution of Washington, 5251 Broad Branch Rd., Washington, D.C. 20015, USA

^c Department of Terrestrial Magnetism, Carnegie Institution of Washington, 5241 Broad Branch Rd., Washington, D.C. 20015, USA

^d School of Earth and Environmental Sciences, Seoul National University, Seoul, 151-747, Republic of Korea

ARTICLE INFO

Article history:

Received 17 June 2007

Received in revised form 7 September 2008

Accepted 22 October 2008

Available online 30 November 2008

Editor: R.D. van der Hilst

Keywords:

serpentine
frictional sliding
earthquake mechanism
acoustic emissions
high pressure
dehydration

ABSTRACT

Using a new four-channel system for detecting acoustic emissions in a multi-anvil apparatus, we have assessed the pressure–temperature range for such emissions, as well as the role of dehydration, by deforming samples of extensively serpentinized peridotite. We show that in the absence of dehydration and for samples initially faulted at low pressure, acoustic emissions occurred well outside the expected pressure–temperature field of unassisted brittle failure. Emissions were also detected during and after dehydration of serpentine. Microstructures of post-run specimens revealed fault slip with offsets up to ~500 μm, regardless of whether or not dehydration took place. Dehydration appears to effectively stop slip on pre-existing faults and create new ones. Analysis of P-wave travel times from the four sensors confirmed that the acoustic emissions originated within the specimen during fault slip. These observations suggest that earthquakes can be triggered by slip along an existing fault containing serpentine under significantly higher pressure and temperature conditions than previously thought possible without dehydration.

© 2008 Elsevier B.V. All rights reserved.

1. Introduction

Because both increasing temperature and pressure favor flow of rocks, earthquakes caused by brittle shear failure or frictional sliding become impossible at great depth in the Earth (Frohlich, 1989; Green and Houston, 1995) unless some additional factor is involved, such as the presence of a pressurized fluid (Scholz, 2002) or a means of producing strength heterogeneity such as a phase transformation (Green and Houston, 1995). The conventional wisdom is that the maximum depth for such unassisted brittle failure or frictional sliding is about 60 km (~2 GPa). At greater depths, however, laboratory experiments suggest that intermediate-depth earthquakes could be triggered by dehydration embrittlement of hydrous minerals such as serpentine (Raleigh and Paterson, 1965; Murrell and Ismail, 1976; Rutter and Brodie, 1988; Meade and Jeanloz, 1991; Green and Houston, 1995; Kirby, 1995; Green and Marone, 2002; Zhao et al., 2002; Dobson et al., 2002; Hacker et al., 2003; Hyndman and Peacock, 2003; Dobson et al., 2004; Jung et al., 2004; Jung and Green, 2004; Green and Jung, 2005), or even dehydration of nominally anhydrous minerals (Zhang

et al., 2004). Recent deformation experiments at high pressure (Jung et al., 2004; Jung and Green, 2004) showed that dehydration of a serpentinized peridotite displayed faults and localized-shear zones independent of the sign of total volume change of reaction, suggesting that dehydration embrittlement of hydrous minerals may be a viable mechanism for triggering earthquakes at any depth, so long as a dehydration reaction can occur.

A critical test for any earthquake mechanism, such as dehydration embrittlement, is to detect acoustic signals when there is an instability in a specimen at high pressure and high temperature, just as one can detect seismic waves from real earthquakes. There have been a few attempts previously to detect acoustic emissions during dehydration of serpentine, with only one or two acoustic sensors (Meade and Jeanloz, 1991; Dobson et al., 2002, 2004), thereby leaving ambiguity in the location of acoustic signals.

Overcoming technical difficulties, Jung et al. (2006) have recently developed a new system for detecting acoustic emissions with 4 channels in a multi-anvil apparatus capable of generating high pressure and high temperature conditions relevant to the upper mantle and transition zone. Each channel has high resolution (12 bit) and a sampling rate of 30 MHz. By conducting experiments at pressures up to 6 GPa and temperatures up to 770 °C, Jung et al. (2006) demonstrated that the new system can be used to detect acoustic emissions under high pressure and temperature conditions. Analyzing acoustic signals with four channels, they were able to show that the new system permits them to distinguish between signal and noise,

* Corresponding author. School of Earth and Environmental Sciences, Seoul National University, Seoul, 151-747, Republic of Korea.

E-mail address: hjung@snu.ac.kr (H. Jung).

¹ Present address: School of Earth and Environmental Sciences, Seoul National University, 311 Ho, 25-1 Dong, San 56-1, Sillim-dong, Gwanak-gu, Seoul, 151-747, Republic of Korea.

and to locate the source of acoustic emissions as being within the sample. Employing this new system, we have examined the mechanical behavior of serpentine at high pressure and temperature including the effect of dehydration.

2. Experimental procedures

Experiments were carried out using a split-cylinder multi-anvil apparatus (at the Geophysical Laboratory of the Carnegie Institution of Washington, D.C.) equipped with a system for detecting acoustic emissions using a sample assembly described in Jung et al. (2006). The sample used in the experiments is an extensively serpentinized peridotite from Val Malenco, Italy, which consists mostly of antigorite serpentine, olivine, and minor magnetite (see fig. 1 of Jung et al., 2004). The specimen was chosen because antigorite has a large stability field at high pressure and high temperature (Ulmer and Trommsdorff, 1995; Wunder and Schreyer, 1997; Stalder and Ulmer, 2001) and the same sample material was used in a previous phase equilibrium study (Ulmer and Trommsdorff, 1995). Our specimens have a diameter of 3.1 mm and a total length of 7.5 mm, and in many cases they were constructed like a stack of coins with a thin Ni layer about 1 μm thick evaporated in high vacuum on the surface of each “coin” for use as a passive marker to quantify fault offset after the experiment (Jung et al., 2004). Fully dense alumina pistons were placed at the top and bottom of the specimen to create a non-hydrostatic stress during pressurization. Temperature was measured with a W5%Re–W26%Re thermocouple located adjacent to the specimen midway between the ends. To minimize temperature gradients in the sample, we used a graphite furnace tapered at both ends. Temperature uncertainties were less than ~ 20 °C between the ends and middle of the sample. Temperature was not corrected for the effect of pressure on the thermocouple electromotive force (emf). Thin Ni foils were also placed at the top and bottom of the sample to fix oxygen fugacity to that of the Ni–NiO buffer. Specimens were examined by back-scattered electron imaging at 20 kV using a scanning electron microscope (SEM Philips XL-30 FEG) equipped with energy-dispersive X-ray spectrometer (E-DAX) at the University of California, Riverside (UCR). Analysis of P-wave travel times from the four sensors was made using the SAC program provided by LLNL.

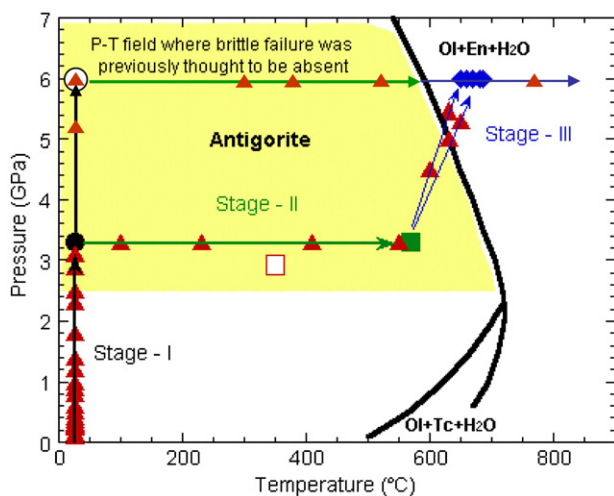


Fig. 1. Stability field of antigorite (Ulmer and Trommsdorff, 1995), experimental conditions and a representative result. Arrows show pressure–temperature paths for experiments shown as three Stages I, II, and III (see text for details). The shaded area shows schematically the pressure–temperature field where brittle failure or frictional sliding was previously thought to be absent. Acoustic emissions (solid triangles) were detected from within specimens during Stage I through the Stage III without/with dehydration of serpentine. White box shows conditions of deformation of serpentinite that did not break (see text). Ol: olivine. Tc: talc. En: enstatite.

We conducted experiments up to $P=6$ GPa and $T=690$ °C that are organized into three stages (Stage I, isothermal compression at room temperature; Stage II, isobaric heating at high pressure; and Stage III, pressurizing and heating simultaneously), as shown in Fig. 1. Fig. 1 shows the stability field of antigorite serpentine with pressure–temperature paths of experiments. The shaded area in Fig. 1 indicates pressure–temperature conditions where frictional sliding was previously thought to be absent because of high pressure, high temperature, and the absence of dehydration reactions. In Stage I, we pressurized specimens at room temperature to $P=3.3$ GPa in 1 h. In Stage II, the specimen was heated to 570 °C over 30 min. In Stage III, both pressure and temperature were increased rapidly at the same time to maintain a non-hydrostatic stress in the specimen and to cross the phase boundary where antigorite breaks down to release H_2O ; during approximately 7 min, pressure was increased to 6 GPa and temperature, to 650–690 °C. Most samples went through all three stages. However, 6 experiments were stopped after Stage I (hereafter referred to as “Stage I experiments”), 7 samples were quenched at the end of Stage II to the apparatus (hereafter referred to as “Stage II experiments”), and one specimen was quenched at $P=4.5$ GPa and $T=600$ °C in the early part of Stage III, where antigorite was still stable. Upon triggering of an event, waveforms of acoustic emissions on all four channels were automatically recorded by a data logger.

3. Results

During Stage I, there were typically 10–20 acoustic emissions (AE) up to ~ 2 GPa, and a few more during further pressurization to $P=3.3$ GPa (solid triangles above ~ 2 GPa in the Stage I, see Fig. 1). Based on the relative travel times of acoustic waves to the 4 transducers, we could determine that some of the AE came from the specimen and others from the surrounding pressure medium (Jung et al., 2006). There was commonly one AE of much larger amplitude (typically $\sim 10\times$) than the others at around 200–300 MPa that we infer was the initial fracture. An example of acoustic emission from the sample at 2.3 GPa in Stage I is shown in Fig. 2a. During heating (Stage II), a few more acoustic emissions (typically 3) were detected from the specimen and likely within the pre-existing fault at temperatures between 60 °C and 570 °C (solid triangles in Stage II, Fig. 1). Note that acoustic emissions were detected in the P – T field where brittle failure/frictional sliding was previously thought to be inhibited (in the shaded area in Fig. 1). An example of acoustic emission from the sample at $P=3.3$ GPa and $T=410$ °C in Stage II is shown in Fig. 2b. During Stage III, acoustic emissions were also observed (Fig. 1) when we increased pressure and temperature simultaneously to the target pressure of 6 GPa and temperatures of 650–690 °C, crossing the dehydration phase boundary of serpentine (Fig. 1). An example of acoustic emission from a sample at 5 GPa and 630 °C in Stage III is shown in Fig. 2c.

Backscattered-electron images of specimen microstructures after the experiments are shown in Fig. 3. The left panel of Fig. 3a shows a typical fault zone of a specimen subjected only to Stage I ($P=3.3$ GPa). The specimen failed by shear fracture during pressurization, yielding a fault with offset of ~ 150 μm , as shown by displacement of a thin Ni layer. Faulting occurs in Stage I experiments because the Al_2O_3 end pieces transmit stress to the specimen that exceeds the failure stress as pressure is increased. Fault sections traversing regions of relict olivine typically show small broken, angular, crystal fragments (Fig. 3a, right panel) typical of both experimental and natural fault gouges (Marone and Scholz, 1989). Virtually all Stage I and Stage II experiments exhibited only one fault; a few showed two faults.

The left panel of Fig. 3b shows a typical fault zone after Stage II ($P=3.3$ GPa, $T=570$ °C). Specimens subjected to both Stage I and Stage II typically showed more slip on the observed faults than specimens that were stopped after Stage I, with a fault offset of ~ 520 μm . Fault zone microstructures are similar to those of Stage I (Fig. 3b, right panel). Examination of Stage I and Stage II fault zones

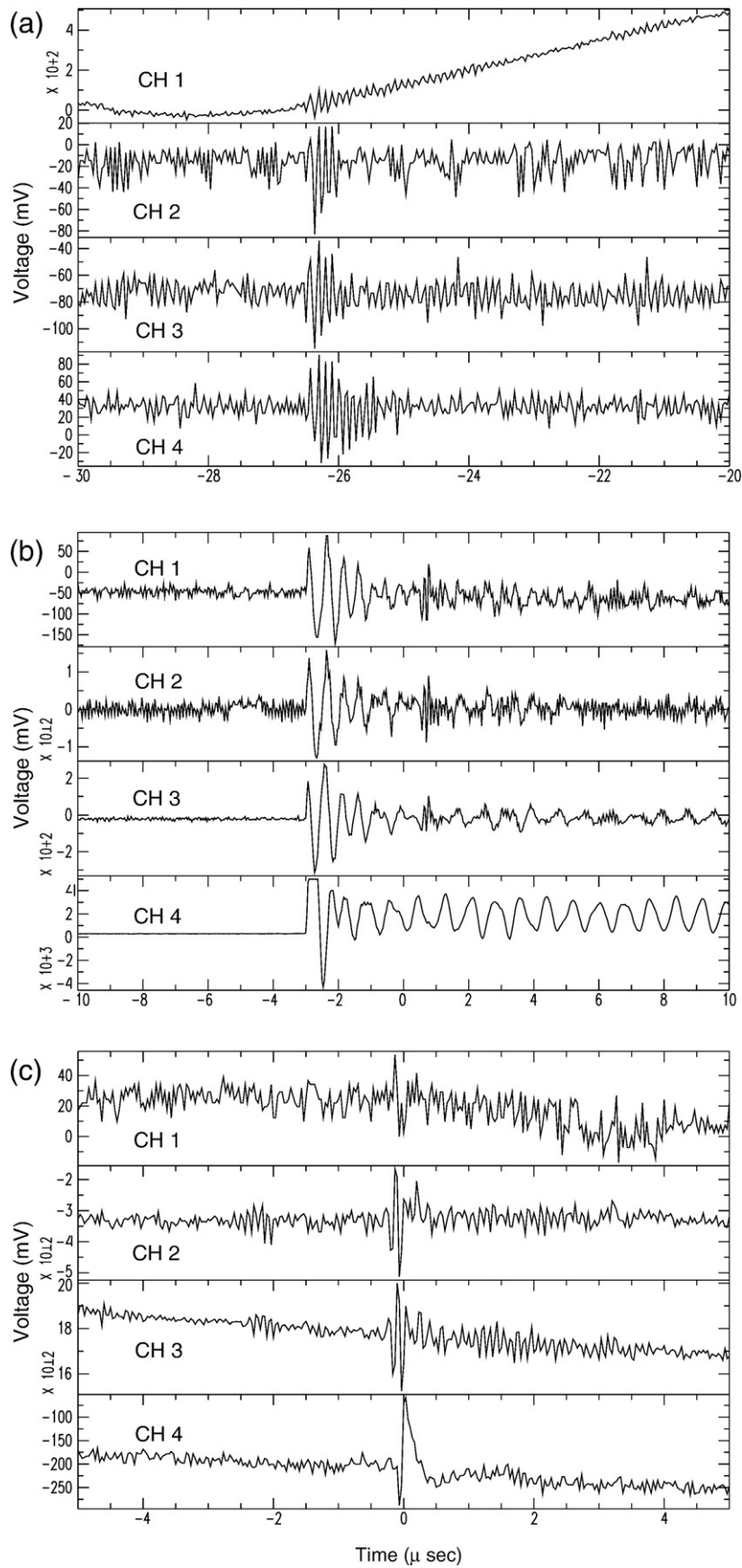


Fig. 2. Acoustic emissions with four channels from specimens in Stage I (a), Stage II (b), and Stage III (c). (a) $P=2.3$ GPa, $T=25$ °C. (b) $P=3.3$ GPa, $T=410$ °C. (c) $P=5.0$ GPa, $T=630$ °C. Travel time differences between the first-arrived and the last-arrived acoustic waves are less than ~ 0.5 μs for (a), (b), and (c), indicating that the source of acoustic emission was from inside of the specimen. This was confirmed by “post-mortem” observation of faults in the appropriate locations within the specimens as shown in Fig. 3.

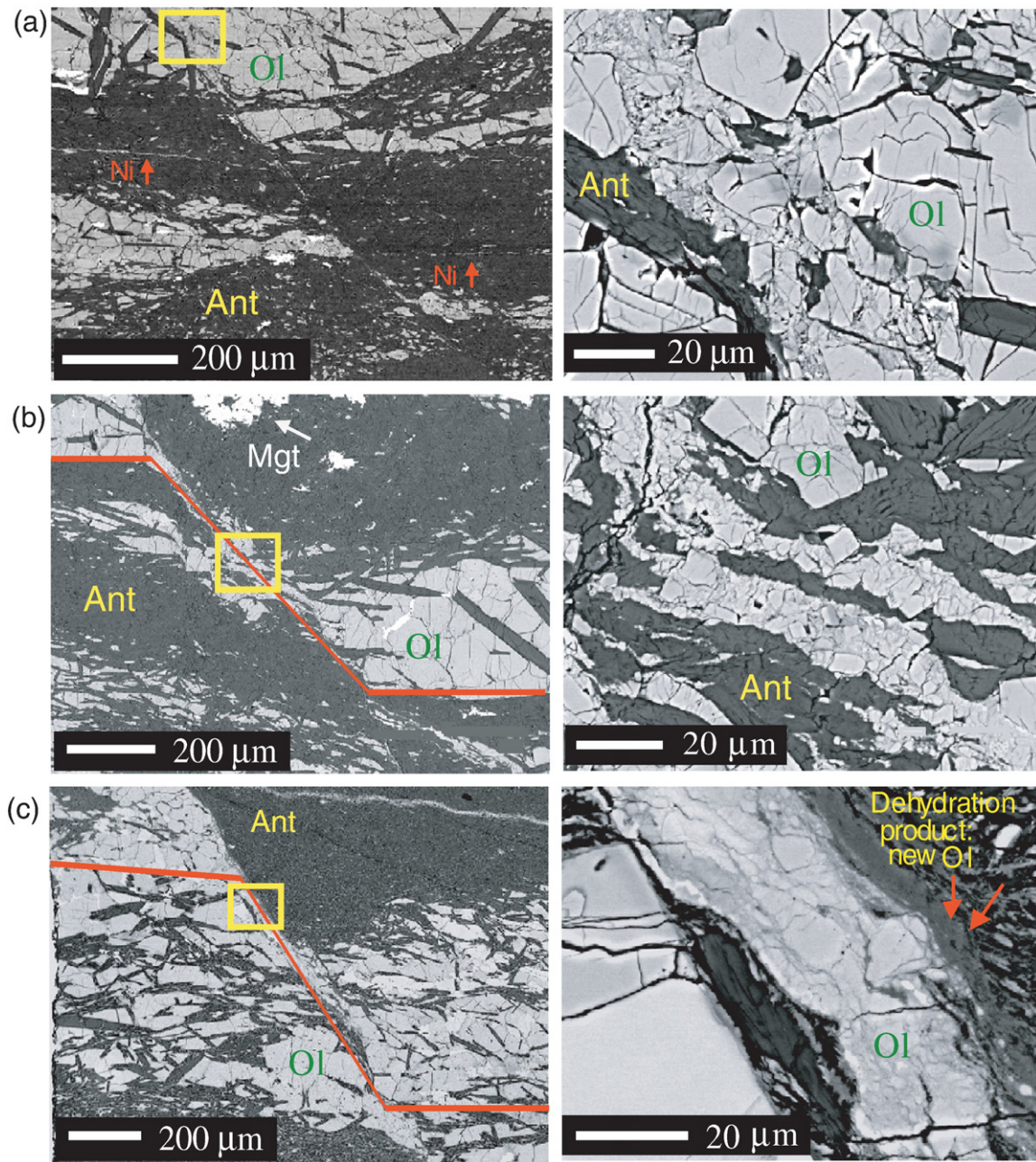


Fig. 3. Backscattered-electron images showing both fault-offset and detailed fault microstructures within experimental specimens in Stage I (a), Stage II (b), and Stage III (c). (a) Left image: sample pressurized to 3.3 GPa at room temperature was faulted with an offset of $\sim 150 \mu\text{m}$ shown by offset Ni markers. Right: magnified view of the inset in the left image showing the small broken-pieces of relict olivine grains. (b) Left: sample quenched at $P=3.3 \text{ GPa}$ and $T=570 \text{ }^\circ\text{C}$ was faulted with an offset of $\sim 520 \mu\text{m}$. Right: magnified view of the inset in the left image showing the small broken pieces of relict olivine grains. Thin red lines were drawn in the left figures of (b) and (c) to show clearly the place of Ni markers, which had weaker contrast in these images than that in (a), but they were clearly visible in higher magnification images. (c) Left: sample showing microstructures after dehydration of serpentine quenched at 6 GPa and $670 \text{ }^\circ\text{C}$. This sample was faulted with an offset of $\sim 550 \mu\text{m}$. Right: magnified view of the inset in the left image showing the small broken-pieces of relict olivine grains along with the dehydration products of serpentine. Ol: olivine. Ant: antigorite. Mgt: magnetite.

between crossed polarizers in the optical microscope revealed that the serpentine in the fault zones was oriented by slip.

The left panel of Fig. 3c shows a typical fault zone after Stage III ($P=6 \text{ GPa}$, $T=670 \text{ }^\circ\text{C}$). Again, the fault offsets ($\sim 550 \mu\text{m}$) tend to be greater than those in Stage I. After dehydration of serpentine during Stage III, the shape of the broken fragments of relict olivine (Fig. 3a,b) become rounded rather than angular and are joined by extremely fine-grained solid reaction products of antigorite dehydration (less than $\sim 300 \text{ nm}$ in diameter), consisting mostly of olivine, but also lesser amounts of enstatite (Fig. 3c, right panel). These reaction products are very similar to those produced previously in failure of intact antigorite during dehydration (Jung et al., 2004).

In order to quantify the fault offsets at different stages, we measured the fault offsets in all experiments. Fig. 4a shows a histogram of fault offsets in the specimens. The fault offsets were determined by measuring offset of Ni layers as shown in backscattered electron images (refer to Fig. 3). Post-run sample analyses after Stage I experiments showed fault offsets in the range of $120\text{--}320 \mu\text{m}$, with a mean value of $190 \mu\text{m}$. Post-run analyses after Stage II experiments showed that only one fault occurred, but with significantly larger slip. Average fault offset after Stage II was $520 \mu\text{m}$. Post-run analyses after Stage III experiments showed a distribution of offsets on the pre-existing fault that was not significantly greater than those in Stage II experiments. The average offset on the pre-existing fault after

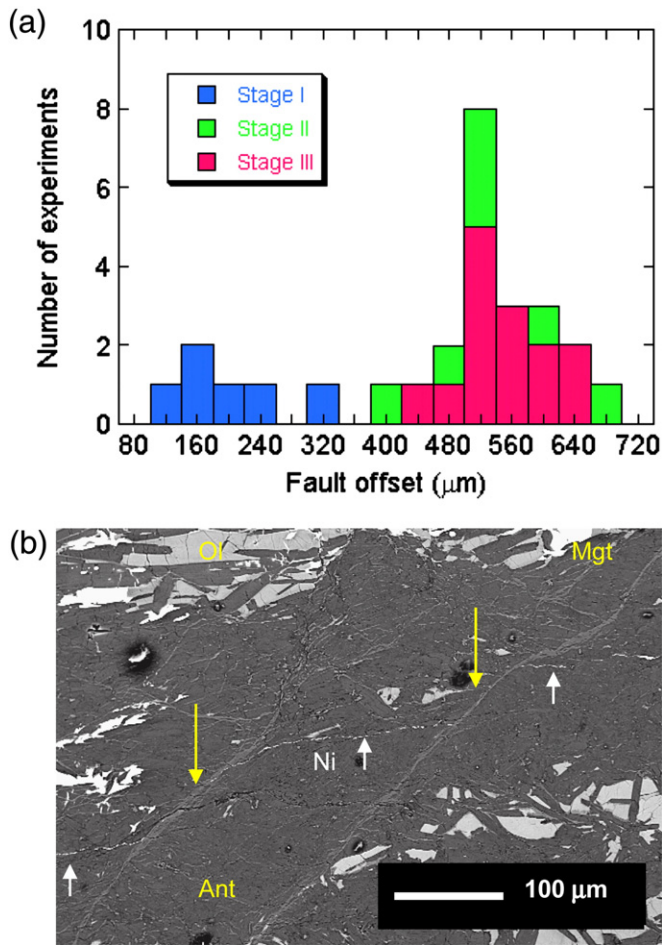


Fig. 4. (a) Number of experiments with fault offset. Fault offsets were measured from the passive Ni markers (see text) in backscattered-electron images. Uncertainty of the measurement of fault offset is less than $\pm 40 \mu\text{m}$. Six samples in Stage I were pressurized to $P=3.3 \text{ GPa}$ at room temperature. Seven samples in Stage II (see Fig. 1) were pressurized to $P=3.3 \text{ GPa}$ and increased temperature to $T=570 \text{ }^\circ\text{C}$. Fourteen samples in Stage III were pressurized to $P=6 \text{ GPa}$ and increased temperature to $T=650\text{--}690 \text{ }^\circ\text{C}$ after following the Stage I and II. This figure clearly shows that there was more fault offset $\sim 300 \mu\text{m}$ along a fault in Stages II and III than that in the Stage I. Also, there is no significant difference in fault offset distribution between Stages II and III. Fault offset associated with dehydration (b) is $\sim 70 \mu\text{m}$ which is off the plot. (b) Small faults during/after dehydration of serpentine in Stage III. Specimens quenched after Stage III typically show additional multiple small faults (see arrows) decorated with dehydration products (gray). Small fault offsets are shown by Ni-markers (arrowheads). This specimen was pressurized to $P=6 \text{ GPa}$ and heated to $T=660 \text{ }^\circ\text{C}$. Ol: olivine. Ant: antigorite. Mgt: magnetite.

dehydration of serpentine in Stage III was $550 \mu\text{m}$. In addition, however, experiments exhibiting dehydration typically showed the creation of multiple new faults with offset typically less than $\sim 100 \mu\text{m}$ (Fig. 4b); the small faults all displayed dehydration products within them.

We also performed eight similar experiments on a synthetic harzburgite (olivine+enstatite) to test whether the observed high-pressure AE were unique to serpentine. As was the case for serpentine, acoustic emissions were observed during pressurization up to 3.3 GPa (Stage I) and heating up to $500 \text{ }^\circ\text{C}$ (Stage II) (Fig. 1), but not upon further heating; faults in harzburgite subjected only to pressurization (Stage I) showed smaller offsets than specimens subsequently heated (Stage II). An additional harzburgite specimen pressurized to 6 GPa at room temperature and then heated to $850 \text{ }^\circ\text{C}$ showed no AE above 3 GPa . These observations showed that acoustic emissions do occur in harzburgite outside the expected P – T range for brittle failure, but they occur in serpentine over a much wider pressure–temperature range.

We conducted two additional experiments on serpentine in which we pressurized to 6 GPa (Fig. 1, white circle). An experiment of pressurization only at room temperature showed AE to 3.3 GPa as described above for Stage I experiments and then at a lower rate all the way to 6 GPa . Stage II and III experiments showed similar AEs to the Stage I that was pressurized to 6 GPa with AEs at $300 \text{ }^\circ\text{C}$, $380 \text{ }^\circ\text{C}$, and $520 \text{ }^\circ\text{C}$ during heating of the specimen in Stage II before dehydration, and 6 GPa and $770 \text{ }^\circ\text{C}$ after dehydration of serpentine (Stage III). After pressurization to 6 GPa , offset on the fault initiated at low pressure was $380 \mu\text{m}$ and after subsequent heating to $850 \text{ }^\circ\text{C}$ was $680 \mu\text{m}$, once again consistent with additional fault offset along the fault after heating the specimen at 6 GPa . As before, dehydration products also were found associated with new faults.

To test whether our observations apply to brittle failure as well as frictional sliding on a pre-existing fault, we deformed a serpentine specimen at 2.8 GPa ; $350 \text{ }^\circ\text{C}$ (open square in Fig. 1b) at a constant strain rate of $2 \times 10^{-4} \text{ s}^{-1}$, using a modified Griggs apparatus (refer to the experimental details in Jung et al., 2004). The sample was not broken, even though the differential stress on the sample reached 3.3 GPa (axial stress = 6.1 GPa), at which point we had to stop the experiment because that corresponded to a stress of 5 GPa on the tungsten carbide piston that applies the stress, near the failure stress of the piston. Post-run examination of the specimen showed no faulting, and there was no detectable deformation of the sample. This observation, along with our observation of a single fault in experiments subjected only to Stage I and Stage II, confirms that frictional sliding occurs at a lower stress than brittle failure and that the acoustic emissions in the latter parts of Stage I and in Stage II are from slipping along a pre-existing fault.

4. Discussion and conclusion

The new and striking result in this study is that we have detected acoustic emissions within specimens at pressures above $\sim 2 \text{ GPa}$ and at temperatures up to $600 \text{ }^\circ\text{C}$ (triangles in the shaded area in Fig. 1). The acoustic signals were detected in Stage I, Stage II, and in the early parts of Stage III, prior to dehydration of serpentine. In most cases, “Post-mortem” examination of specimens revealed only one fault in specimens subjected only to Stage I or to Stages I and II, with progressively more fault offset (no dehydration). The absence of other faults strongly suggests that the acoustic emissions occurred on this single fault. We thus conclude that these faults were created by brittle shear fracture during Stage I, and that the observed acoustic emissions during Stage II and the early stages of Stage III were due to repeated frictional sliding on existing faults.

It is striking that, within the measurement error, dehydration produced no further slip on pre-existing faults but numerous new faults (Fig. 4b). This suggests that dehydration-induced faulting occurs at a lower stress than frictional sliding under these conditions. It is not clear why this should happen preferentially on new faults; we speculate that the pre-existing faults contained some uncollapsed pore volume such that dehydration would have less pore-pressure effect than in new faults formed in fully-dense material.

The experiments in this study raise two basic questions. First, is the level of frictional stress during fault slip sufficiently low to be relevant to natural faults in the subducted slab? Second, what physical mechanism could account for these observations? Regarding the first question, we are particularly interested in stresses at elevated confining pressure, and at elevated temperature, beyond the conventional brittle field. We can obtain an upper bound for the frictional stress, σ_f , on a preexisting fault through the expected frictional heat generation and resulting increase in temperature, ΔT , $\Delta T = \sigma_f D / \Delta d c \rho$, (Kanamori et al., 1998) where D is the amount of fault slip during an event, c is specific heat, and ρ is density. Δd is the thickness of the layer being heated: either the thickness of the fault zone, $10 \mu\text{m}$ in our case, or the thermal diffusion length scale, L , whichever is larger. Since $L \sim (k\tau)^{1/2}$, where k is the thermal diffusivity and τ is the slip duration,

L will be no greater than $10\ \mu\text{m}$ as long as τ is less than $100\ \mu\text{s}$. The seismograms in Fig. 2 suggest much shorter durations of a few μs . Thus, taking $\Delta d=10\ \mu\text{m}$, $D=25\text{--}100\ \mu\text{m}$ (1–4 slip events during Stage II), $c=10^3\ \text{J/kg}\ ^\circ\text{C}$, $\rho=3\times 10^3\ \text{kg/M}^3$, then $\Delta T=K\sigma_f$, where $K\sim 1\ ^\circ\text{C/MPa}$. Previous deformation experiments using the same serpentinite showed that in the absence of preexisting faults, differential stress was a large fraction of the confining pressure (Jung et al., 2004). If we assume this is the case for our experiment, and using a frictional stress of 1 GPa, the corresponding temperature rising from frictional heating would be about $1000\ ^\circ\text{C}$. But the absence of any dehydration products in Stage I or II requires that the temperature in the fault zone be less than the temperature of the dehydration phase boundary, $\sim 650\ ^\circ\text{C}$. Because we have AE up to $T\sim 550\ ^\circ\text{C}$, the temperature rise from frictional heating can be no more than about $100\text{--}200\ ^\circ\text{C}$, thus bounding frictional stress to be no more than about 100 MPa. This level of frictional stress is comparable to that inferred for some earthquakes at high pressure (Kanamori et al., 1998), and is thus a stress level that is relevant for subducting lithosphere.

To address the question of the physical mechanism, we started with the general observations, including (i) acoustic emissions caused by frictional sliding on existing faults at high pressure and temperature in serpentinite up to 6 GPa and $550\ ^\circ\text{C}$ (pre-dehydration) as well as in harzburgite, but only up to 3.3 GPa and $500\ ^\circ\text{C}$, (ii) no faulting in serpentinite at high pressure if existing faults are not present, (iii) creation of new faults from dehydration in serpentinite, and (iv) cessation of faulting on preexisting faults once dehydration occurs. No evidence for melting (or dehydration) is found during brittle failure of virgin material in either serpentinite or harzburgite (or any other materials), even in cases where the differential stress at failure is in excess of 1 GPa (Scholz, 2002; Jung et al., 2004). Based upon these observations, we propose the following physical explanation for our experiments: (i) AE occurring at room temperature and low pressure are the result of brittle failure accompanied by significant dilation within the fault zone and repeated slip on that fault zone, analogous to initial failure and sliding in brittle-failure experiments (Jung et al., 2004); (ii) AE during subsequent heating results from fault slip equivalent to aftershocks on natural faults and is the result of failure of local asperities on a weakened and porous fault zone; and (iii) initia-

tion of new faults upon dehydration arises from rapid rise of fluid pressure on new embryonic faults, resulting in abandonment of pre-existing faults where the presence of residual porosity reduces the pore-pressure-raising effect of dehydration. This scenario is also consistent with our observations that AE is reduced by further pressurization to 6 GPa (reduction of porosity in the gouge by compaction) and the differences in AE behavior between serpentinite and harzburgite. Raising the pressure from 3 to 6 GPa will significantly reduce the porosity within the fault zone by compaction, inhibiting the “aftershock” effect as observed following earthquakes at intermediate depths (Persh and Houston, 2004). The increase in pressure will more effectively inhibit slip on faults in harzburgite because compaction will return the material to approximately its virgin strength. In contrast, fault slip in serpentinite progressively orients serpentine in the fault zones as found here (Fig. 5) and previously (Escartin et al., 1997), rendering them progressively weaker due to plasticity and thereby partially compensating for the compaction effect and enabling fault slip even at 6 GPa.

The results of our experiments may shed light on the general lack of evidence of high temperatures after slip on natural faults. The simple calculations above would predict extensive melting unless frictional stress on the fault plane is dramatically lower than the differential stresses. Our interpretation that porosity generation plays an important role during faulting and sliding suggests that fault-strength heterogeneity may be the key. In particular, in a porous fault zone, where the strength of the fault is controlled by a few high-strength asperities, then the localized flash dehydration (melting) of these asperities could occur, leading to a rapid drop of overall fault strength, without generating a large amount of heat. Indeed, this particular weakening mechanism has been recently proposed to account for the absence of melting accompanying earthquakes on very thin, mature faults at shallow depths (Rice, 2006). We propose that this same mechanism may extend to deep events.

One of the outstanding questions concerning earthquakes in subduction zones concerns where frictional sliding earthquakes end and other mechanism(s) take over. Strong evidence has recently been reported suggesting that dehydration reactions within the subducting oceanic crust are important for initiating earthquakes at depths of

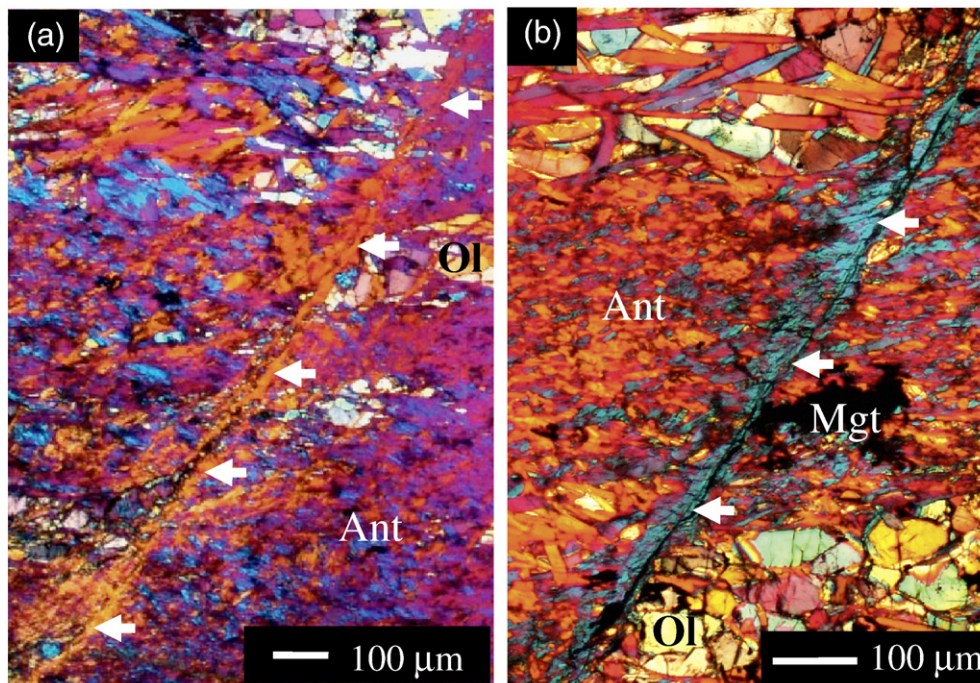


Fig. 5. Optical photomicrograph with transmitted light showing antigorite aligned along faults in serpentinite. (a) Sample after Stage I ($P=3.3\ \text{GPa}$, $T=25\ ^\circ\text{C}$). (b) Sample after Stage II ($P=3.3\ \text{GPa}$, $T=570\ ^\circ\text{C}$). White arrows show antigorite crystals strongly aligned with their cleavage planes in the fault. Ol: olivine. Ant: antigorite. Mgt: magnetite.

70–120 km or so beneath Japan (Kita et al., 2006), at which point the earthquakes migrate into the mantle portion of the slab. However, Japan and most other subduction zones exhibit double seismic zones in the depth range ~50–250 km; the lower zone is in the mantle and the potential origin of these earthquakes remains controversial (Green and Houston, 1995; Silver et al., 1995; Green and Marone, 2002). A significant implication of this acoustic emission study is that frictional sliding on existing faults may explain many of the earthquakes in the lower zone, especially in the presence of serpentine, to depths approaching 200 km, depending on the temperature.

Acknowledgements

We thank L. F. Dobrzhinetskaya, G. Gudfinnsson, C. Hadidiacos, W. Jiao, D. Oglesby and J. Zhang for helpful discussions and technical support, and F. Forgit for specimen assembly preparation and laboratory assistance. This work was supported by NSF grants to HWG and YF, and by Grant CATER 2008–5112 (HJ) and BK21 at SEES, SNU (HJ), and the Carnegie Institution of Washington.

References

- Dobson, D.P., Meredith, P.G., Boon, S.A., 2002. Simulation of subduction zone seismicity by dehydration of serpentine. *Science* 298, 1407–1410.
- Dobson, D.P., Meredith, P.G., Boon, S.A., 2004. Detection and analysis of microseismicity in multi anvil experiments. *Phys. Earth Planet. Inter.* 143–144, 337–346.
- Escartin, J., Hirth, G., Evans, B., 1997. Nondilatant brittle deformation of serpentinites: implications for Mohr–Coulomb theory and the strength of faults. *J. Geophys. Res.* 102, 2897–2913.
- Frohlich, C., 1989. The nature of deep-focus earthquakes. *Ann. Rev. Earth Sci.* 17, 227–254.
- Green, H.W., Houston, H., 1995. The mechanics of deep earthquakes. *Annu. Rev. Earth Planet. Sci.* 23, 169–213.
- Green, H.W., Jung, H., 2005. Fluids, faulting and flow. *Elements* 1, 31–37.
- Green, H.W., Marone, C., 2002. Instability of deformation. In: Karato, S., Wenk, H.-R. (Eds.), *Plastic Deformation of Minerals and Rocks. Reviews in Mineralogy and Geochemistry*, vol. 51, pp. 181–199.
- Hacker, B.R., Peacock, S., Abers, G.A., Holloway, S.D., 2003. Subduction factory 2. Are intermediate-depth earthquakes in subducting slabs linked to metamorphic dehydration reactions? *J. Geophys. Res.* 108 (B1), 2030. doi:10.1029/2001JB001129.
- Hyndman, R.D., Peacock, S.M., 2003. Serpentinization of forarc mantle. *Earth Planet. Sci. Lett.* 212, 417–432.
- Jung, H., Green, H.W., 2004. Experimental faulting of serpentinite during dehydration: implications for earthquakes, seismic low velocity zones, and anomalous hypocenter distributions in subduction zones. *Int. Geol. Rev.* 46, 1089–1102.
- Jung, H., Green, H.W., Dobrzhinetskaya, L.F., 2004. Intermediate-depth earthquake faulting by dehydration embrittlement with negative volume change. *Nature* 428, 545–549.
- Jung, H., Fei, Y., Silver, P.G., Green, H.W., 2006. System for detecting acoustic emissions in the multianvil experiments: application to deep seismicity in the earth. *Rev. Sci. Instrum.* 77, 014501–1–014501-7.
- Kanamori, H., Anderson, D.L., Heaton, T.H., 1998. Frictional melting during the rupture of the 1994 Bolivian earthquake. *Science* 279, 839–842.
- Kirby, S., 1995. Intraslab earthquakes and phase changes in subducting lithosphere. *Rev. Geophys.* 33 (Suppl.), 287–297.
- Kita, S., Okada, T., Nakajima, J., Matsuzawa, T., Hasegawa, A., 2006. Existence of a seismic belt in the upper plane of the double seismic zone extending in the along-arc direction at depths of 70–100 km beneath NE Japan. *Geophys. Res. Lett.* 33, L24310. doi:10.1029/2006GL028239.
- Marone, C., Scholz, C.H., 1989. Particle-size distribution and microstructures within simulated fault gouge. *J. Struct. Geol.* 11 (7), 799–814.
- Meade, C., Jeanloz, R., 1991. Deep-focus earthquakes and recycling of water into the earth's mantle. *Science* 252, 68–72.
- Murrell, S.A.F., Ismail, I.A.H., 1976. The effect of decomposition of hydrous minerals on the mechanical properties of rocks at high pressures and temperatures. *Tectonophysics* 31, 207–258.
- Persh, S.E., Houston, H., 2004. Strongly depth-dependent aftershock production in deep earthquakes. *Bull. Seismol. Soc. Am.* 94, 1808–1816.
- Raleigh, C.B., Paterson, M.S., 1965. Experimental deformation of serpentinite and its tectonic implications. *J. Geophys. Res.* 70, 3965–3985.
- Rice, J.R., 2006. Heating and weakening of faults during earthquake slip. *J. Geophys. Res.* 111, B05311. doi:10.1029/2005JB004006.
- Rutter, E.H., Brodie, K.H., 1988. Experimental “syntectonic” dehydration of serpentinite under conditions of controlled pore water pressure. *J. Geophys. Res.* 93, 4907–4932.
- Scholz, C.H., 2002. *The Mechanics of Earthquakes and Faulting*. Cambridge University Press.
- Silver, P.G., Beck, S.L., Wallace, T.C., Meade, C., Myers, S.C., James, D.E., Kuehnel, R., 1995. Rupture characteristics of the deep Bolivian earthquake of 9 June 1994 and the mechanism of deep-focus earthquakes. *Science* 268, 69–73.
- Stalder, R., Ulmer, P., 2001. Phase relations of a serpentine composition between 5 and 14 GPa: significance of clinohumite and phase E as water carriers into the transition zone. *Contrib. Mineral. Petrol.* 140, 670–679.
- Ulmer, P., Trommsdorff, V., 1995. Serpentine stability to mantle depths and subduction related magmatism. *Science* 268, 858–861.
- Wunder, B., Schreyer, W., 1997. Antigorite: high pressure stability in the system MgO–SiO₂–H₂O (MSH). *Lithos* 41, 213–227.
- Zhang, J., Green, H.W., Bozhilov, K., Jin, Z., 2004. Faulting induced by precipitation of water at grain boundaries in hot subducting oceanic crust. *Nature* 428, 633–636.
- Zhao, D., Mishra, O.P., Sanda, R., 2002. Influence of fluids and magma on earthquakes: seismological evidence. *Phys. Earth. Planet. Int.* 132, 249–267.